Quality Control and Tilt Correction Effects on the Turbulent Fluxes Observed at an Ocean Platform

HYUN-MI OH

Division of Earth Environmental System, Pusan National University, Busan, South Korea

KYUNG-EAK KIM

Department of Astronomy and Atmospheric Sciences, Kyungpook National University, Daegu, South Korea

KYUNG-JA HA

Division of Earth Environmental System, Pusan National University, Busan, South Korea

LARRY MAHRT

College of Oceanic and Atmospheric Science, Oregon State University Corvallis, Oregon

JAE-SEOL SHIM

Coastal Disaster Prevention Research Division, Korea Ocean Research and Development Institute, Ansan, South Korea

(Manuscript received 7 August 2009, in final form 30 July 2010)

ABSTRACT

This study investigates atmospheric factors influencing the quality and the postprocessing (e.g., tilt correction) of fast-response measurements of turbulent fluxes for difficult open-sea measurements over an offshore platform. The data were collected at the Ieodo Ocean Research Station over the Yellow Sea during the period from 5 November 2007 to 19 February 2008. The quality control removal of the data generally depends on wind speed, relative humidity, significant wave height, visibility, and stability. The removal of substantial water vapor data with weak-wind stable conditions is investigated. Three different tilt correction algorithms (double rotation, triple rotation, and planar fit) are applied to correct the data because of inadvertent tilt of sonic anemometers. The choice of tilt correction method significantly influences the angle between the wind and stress direction.

1. Introduction

More than 70% of the earth's surface is covered with oceans. To understand the physical processes related to atmosphere–ocean interaction, flux measurements over the ocean are necessary. Because of insufficient direct observations of fluxes over the sea surface, air–sea fluxes in models have often been parameterized in terms of mean parameters and the bulk exchange coefficient. The parameterizations are based on the results of field experiments conducted over land and sea. While a number of long-term flux measurements are available from towers in the coastal zone, long-term flux measurements are not readily available over the open ocean. The present study examines such observations taken from an open ocean research station.

Before air–sea fluxes can be used with confidence, postprocessing, including quality control and tilt correction, needs to be applied. Because of a minimal history of collecting fast-response data from an open ocean platform, the postprocessing is not a routine procedure and must be investigated in some detail, particularly because of instrument problems due to intense sea fog in weak-wind conditions and sea spray and salt contamination in strong-wind conditions. In addition, flow distortion by offshore

Corresponding author address: Kyung-Ja Ha, Division of Earth Environmental System, Pusan National University, Busan, 609-735, South Korea.
E-mail: kjha@pusan.ac.kr

DOI: 10.1175/2010JAMC2367.1

© 2011 American Meteorological Society

platforms may be substantial. While corrections of unknown generality are possible for mild flow distortion (e.g., Kraan and Oost 1989), flow distortion is problematic if enhanced shear due to the distortion increases shear generation of turbulence. In this case, reliable correction methods are unavailable and may be unattainable.

Since manual quality control of large datasets is laborious, a number of automated methods have been developed (e.g., Højstrup 1993; Foken and Wichura 1996; Vickers and Mahrt 1997). Mauder et al. (2007) recently estimated latent and sensible heat fluxes by applying post–field data-processing methods in an energy balance experiment. Intercomparison of six different post–field data-processing methods showed differences of 15% for the latent heat flux and 10% for the sensible heat flux. Their study indicates that the estimation of both latent and sensible heat fluxes depend significantly on the type of the postprocessing.

The tilt correction is applied to remove the influences of flow distortion induced by the instrument, support bracket, and platform. The tilt correction also removes the influence of inadvertent tilt of the anemometer on the wind components. Tanner and Thurtell (1969) developed a tilt correction method (double rotation method) in which the condition of $\overline{v} = 0$ (first rotation) and $\overline{w} = 0$ (second rotation) must be satisfied for every averaging period (u, v, and w, are the longitudinal, lateral, and vertical velocity components, respectively). Subsequently, a number of tilt correction methods have been developed (McMillen 1988; Kaimal and Finnigan 1994; Paw U et al. 2000; Wilczak et al. 2001; Finnigan et al. 2003). McMillen (1988) suggested a third rotation ($\overline{v'w'} = 0$) for flux data observed over complex terrain. The quantity ($\overline{v'w'}$) is the lateral stress component. However, the tilt correction by both double and triple rotation is still incomplete; the double rotation does not remove the influence of tilt perpendicular to the mean wind, while the third rotation ($\overline{v'w'} = 0$) eliminates any real lateral stress. Such lateral stress can be significant over the sea, as discussed below.

Both double and triple rotations can remove real vertical motion, particularly because they are applied to short time periods, such as 30 min or 1 h. Wilczak et al. (2001) developed an efficient tilt correction method–planar fit method that reduces such problems. This method derives the rotation angles using all of the data in a field program to reduce run-to-run stress errors. The planar fit method determine "tilt angle" for a set of data runs (several weeks or more with no movement of sonic anemometer). Since many data runs are used to determine the tilt angles, it is much less susceptible to sampling errors. The disadvantage of the planar fit is that it does not conserve kinetic energy (Sun 2007) and is not amenable to correction for flow distortion characterized by more complex dependence on wind direction. Offshore platforms may induce substantially more flow distortion than land-based towers. Ocean-based platforms are generally more bulky than towers over land. More complex direction dependence is accommodated by applying the double rotation methods to different wind direction groups using data for an entire field program, but this approach still neglects the influence of tilt rotation perpendicular to the wind direction. The influences of sonic anemometer tilt and flow distortion due to the transducers, support brackets, and platform are difficult to separate. Yim et al. (2006) suggested utilizing a direction without flow distortion by applying the computational fluid dynamics technique. Unfortunately, this technique is difficult to apply to actual geophysical situations.

The Ieodo Ocean Research Station (IORS) was constructed by the South Korean government in 2003 to observe the oceanic environment of East Asia. Since then, unique open ocean atmospheric, oceanic, and environmental data have been collected. They include turbulence data from sonic anemometers, visibility, precipitation, and wave height. However, the potential impact of flow distortion from the platform, as well as other open-sea influences such as sea spray, requires more analysis.

The objective of the present study is to investigate how atmospheric and oceanic conditions affect the errors in the fast-response data and to evaluate different characteristics of tilt correction methods. To what degree do errors occur more often under certain conditions, creating a bias? Can the angle between the wind and stress direction be adequately estimated, or are such estimates too sensitive to the choice of tilt correction method? As a physical application, we study the influence of the tilt correction on the angle between the wind and stress vectors. While the bulk formula and Monin–Obukhov similarity theory assume that the stress and wind direction are aligned, a number of processes lead to nonalignment (e.g., Friehe et al. 1996; Geernaert 1983; Grachev et al. 2003, and references therein). We describe the measurement and the observational data in section 2. The postprocessing is detailed in section 3. The effects due to quality control and tilt correction methods are presented in section 4. Our conclusions are summarized in section 5.

2. Data and analysis methods

IORS (Korea Ocean Research and Development Institute 2001) is constructed on Ieodo, a large underwater rock found in the East China Sea (32.12°N, 125.18°E). It is located 149 km southwest from Marado, the southernmost island of South Korea. IORS (Fig. 1) is an open-sea station with no orographic influence from the southwestern part of the Korean Peninsula. IORS has operated

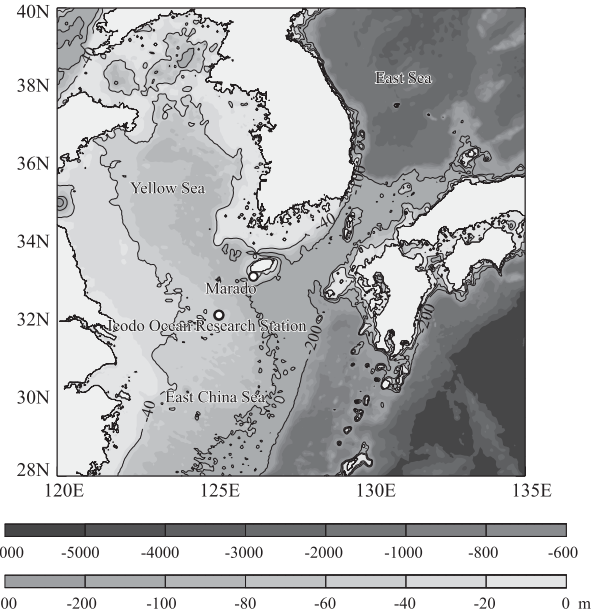

FIG. 1. Location of IORS. Gray shading indicates water depth. IORS is constructed on the underwater rock Ieodo in the East China Sea (32.12°N, 125.18°E). The depths of −40, −100, and −200 m are indicated as contours. The depth of the water around IORS is about 40 m.

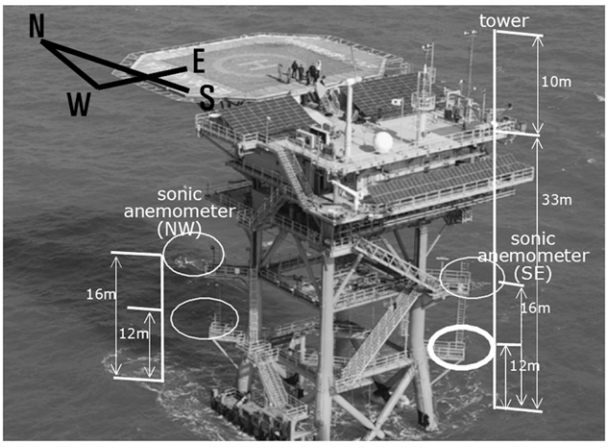

FIG. 2. The IORS. The height of the platform deck is 33 m above mean sea level. The meteorological tower is located 10 m above the platform deck. The sonic anemometer is installed on the boom of the pillar under the deck at a height of 16 and 12 m from mean sea level. The circles show position of the sonic anemometer. The sonic anemometer faces NW during wintertime and SE during the summertime. The thick circle indicates the system observed the data used in this paper (12 m, SE).

since May 2003. The depth of the water around IORS is about 40 m. Most ocean platforms are constructed near coastal region for convenient management (Johansson et al. 2001; Pospelov et al. 2009). IORS is well situated for measurement of southwestern monsoon flow during the boreal summer and winter seasons. As shown in the Fig. 2, the meteorological tower is deployed at a height of about 10 m above the floor of the upper level of the platform.

Velocity and temperature fluctuations were measured with a Campbell CSAT3 3D sonic anemometer, while moisture fluctuations were measured with a LiCor Inc. LI-7500 open path gas analyzer. The characteristics of the CSAT3 and the LI-7500 are documented in Foken et al. (1997) and Foken (1999). This system is often used as a reference instrument in intercomparison experiments (Mauder et al. 2006; Mauder et al. 2007). The CSAT3 and the LI-7500 are installed on the boom of the pillar under the deck at a height of 16 and 12 m from mean sea level. The installed direction of sonic anemometer alternates between the northwestern (NW) and the southeastern (SE). The measurement heights are 12 and 16 m in each direction. In this paper, we analyze the data collected at 12-m height on a 2-m boom directed toward the southeast (Fig. 2) from 5 November 2007 to 19 February 2008. The recording speed of the fast-response data is 10 Hz. The turbulent fluxes are calculated using a constant 30-min averaging time. Atmospheric, oceanic, and environmental data including wind, temperature, humidity, pressure, solar insolation, visibility, rainfall, significant wave height, and seawater temperature (−10 m) have been compiled regularly since 2004. These variables are recorded at 10-min intervals. Additional meteorological data observed at the tower and oceanic data are also used.

In this investigation, the postprocessing on flux data is composed of two steps: the quality control process and the tilt correction process. Details of the postprocessing are explained in the next section. In the analysis of quality control, observation errors are flagged as hard (definite error) and soft (possible error). Flagging ratios and removal ratios for these errors will be examined in relation to prevailing conditions, such as horizontal wind speed, relative humidity, significant wave height, visibility, and stability parameter. Three tilt correction methods are evaluated through comparison of the angle between the stress vector and the wind direction, stress vectors, turbulent fluxes.

3. Quality control

a. Steps of quality control

Prior to the application of quality control, approximately 49.7% of the records are eliminated because the horizontal wind direction is between 270° and 360° and thus affected by platform flow distortion. The quality control and postprocessing of 30-min records (Fig. 3) consist of a weather check, the quality control algorithm of Vickers and Mahrt (1997, called VM checks), flag check, direction check, and

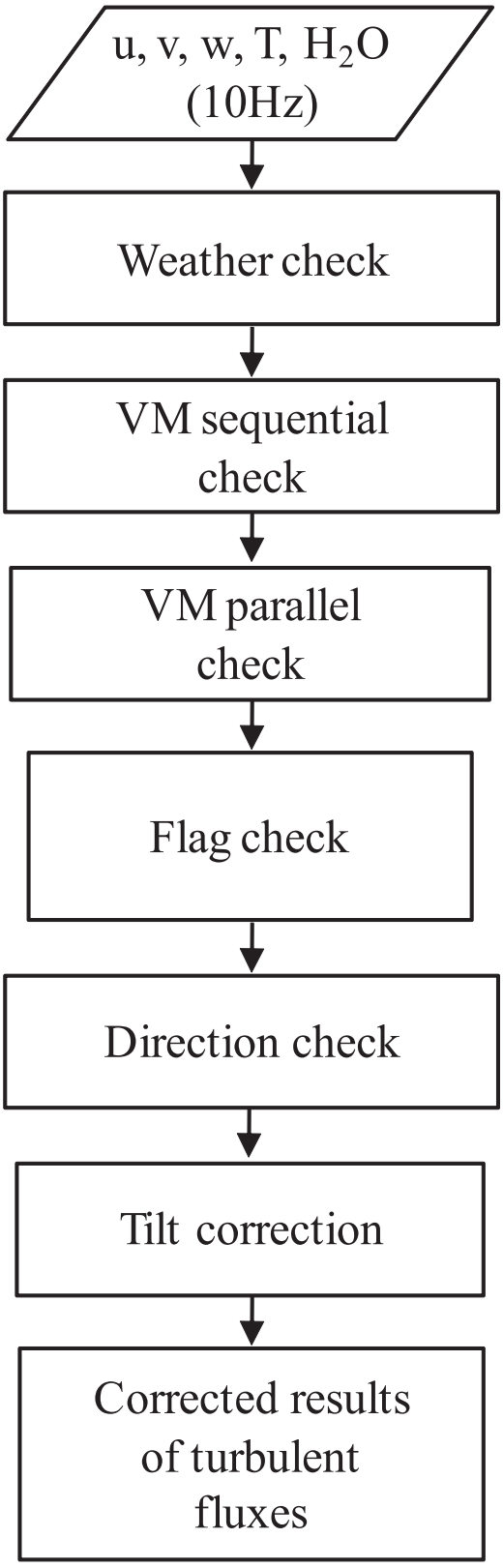

FIG. 3. Schematic diagram of the postprocessing for the fast-response data.

TABLE 1. Criteria of range check for observed variables.

Variable	Criteria
u wind (u)	± 30 m s^{-1}
v wind (v)	± 30 m s^{-1}
w wind (w)	± 5 m s^{-1}
Temperature	$-10°$ to 40°C
Water vapor	0–50 g m^{-3}

tilt correction. The weather check eliminates errors associated with rainfall or fog condensation. Data are omitted if there is any recorded rainfall, visibility is less than 2 km, or when relative humidity is greater than 85%. These criteria attempt to prescreen for the potential of condensation or water drops on the transducers, and water vapor window.

As a second step, we apply the VM tests. The tests for abnormal range of values and spike are performed sequentially (VM sequential checks). The VM sequential checks are designed to identify serious error induced by instrumental problems. So, hard flags are raised during the VM sequential checks; the criteria for the range checks are listed in Table 1. The criteria are suggested in Vickers and Mahrt (1997). The values beyond the criteria for the range check are replaced by missing values. These values are caused by serious instrumental problems. The spikes occur because of electronic problems, with most spikes caused by water droplets. When water droplets impact the surface of the transducer, the heat transfer rate increases and voltage spike occurs (Thomson and Hassman 2001). Any point that is more than 3.5 standard deviations from the mean is detected as a spike where the mean is computed over a 5-min moving window. The spike is replaced by a linearly interpolated value. When the number of spikes detected is greater than 1% of the total data points, the record is hard flagged and eliminated.

The amplitude resolution, skewness and kurtosis, Haar mean and variance, and dropout are performed in parallel (VM parallel checks). The amplitude resolution estimates whether the resolution is sufficient to capture the turbulent fluctuations. Dropouts are defined when sequential points are ''stuck'' at a constant value. Skewness and kurtosis of the data are used to detect instrumental or recording problem. Haar mean and variance estimate discontinuity of data (Mahrt 1991). We use the criteria for the VM parallel checks suggested in Vickers and Mahrt (1997). The VM sequential checks are designed to identify serious error induced by instrumental problems. So, hard-flagged data are raised during the VM sequential checks. After the VM sequential checks are performed, the VM parallel checks are used to determine hard or soft flags. These flags identified by this step are used in the flag check step. When the total number of hard flags within a

TABLE 2. Percentage of records of each variable for soft and hard flags for each process step.

Step of process	Variable	Soft	Hard
Absolute limits	u, v		0.9
	w		2.4
	Temperature		1.0
	Water vapor		10.5
Amplitude resolution	u, v		0.0
	w		0.0
	Temperature		3.3
	Water vapor		0.8
Spike	u, v		0.0
	w		0.0
	Temperature		0.0
	Water vapor		0.1
Dropouts	u, v		0.1
	w		2.0
	Temperature		2.1
	Water vapor		11.0
Skewness	u, v	0.7	0.0
	w	0.1	0.1
	Temperature	6.8	0.3
	Water vapor	13.0	6.3
Kurtosis	u, v	0.1	0.0
	w	0.3	0.3
	Temperature	1.1	0.4
	Water vapor	6.0	6.5
Haar mean	u, v	0.2	0.0
	w	0.7	4.3
	Temperature	0.4	0.7
	Water vapor	0.9	9.3
Haar variance	u, v	0.0	0.0
	w	5.0	0.0
	Temperature	0.7	0.0
	Water vapor	9.0	0.0

30-min record is two or more, the record is permanently removed in this step.

Table 2 shows percentage of records (whole data period) of each variable for soft and hard flags for each VM checks step. The absolute limit is flagged in 0.9%–10.5% of the records. The water vapor data is eliminated 0.1% in the spike step. Air temperature is flagged most frequently in the step of the amplitude resolution. Most of the data with serious contamination are flagged multiple times in the VM parallel checks. Water vapor is flagged most frequently in the quality control procedure. Water vapor is hard flagged in approximately 11% of the entire dataset, while other variables are flagged in 0.1%–4.3%. Other results are summarized in Table 2. The removal ratio in the whole quality control process (in percentage) is 1.6% for the u component, 2% for the v component, 7.2% for the w wind, 2.4% for air temperature, and 15.2% for water vapor.

b. Results of quality control

We now analyze the relationship between the error flag ratio and meteorological and oceanic variables. The soft- (hard-) flag ratio is defined as the ratio of whole data on which was performed the weather check to the soft- (hard-) flagged data. Figure 4 shows the error flag ratio of water vapor as a function of horizontal wind speed, relative humidity, significant wave height, and visibility. For weak winds (<3 m s^{-1}), the error ratio increases with decreasing wind speed. The hard-flag ratio for the lowest wind speed category is about 20% (Fig. 4a). Since cases of fog formation should have been eliminated by the weather checks above, the reason for the increasing flagging at weak winds is not known.

For strong winds (>15 m s^{-1}), the hard-flag ratio rapidly increases with wind speed, probably because of sea spray, and is as high as 40% at 17 m s^{-1}. The soft-flag ratio shows similar dependence on wind speed. The hard flag ratio increases with relative humidity to about 20% (Fig. 4b), with an opposite trend for soft flags. In Fig. 4c, the distribution of the error flag ratio as a function of significant wave height is similar to that for horizontal wind speed. This reflects the close correlation between significant wave height and horizontal wind speed (Kinsman 1965; Carter 1982; Tucker and Pitt 2001). As shown in Fig. 4d, the hard-flag ratio generally increases with decreasing visibility when visibility is less than 10 km. The visibility check may have been too lenient; however, stricter criteria would have eliminated too many good (physically meaningful) records. When visibility is 3 km, the hard-flag ratio is up to 35%. It may be that condensation remains a problem for a finite time period after fog condensation and rain terminates when winds are weak and the relative humidity is high.

Figure 5 shows the error-flag ratio for the vertical velocity component. For the vertical velocity component from the sonic anemometer, the hard- and soft-flag ratios increase rapidly with strong winds reaching 20% when the wind speed exceeds 15 m s^{-1} (Fig. 5a). Flag ratios do not show any correlation with the relative humidity (Fig. 5b). The hard-flag ratio slightly increases when the significant wave height is low (Fig. 5c). The hard-flag ratio also slightly increases when the visibility is low (Fig. 5c). Figure 6a shows the total removal ratio due to all of the steps for the wind components, air temperature, and water vapor as a function of horizontal wind speed. The total removal ratio is defined as the ratio of whole data to removed data in all of the steps. The other panels in Fig. 6 show the total removal ratio as a function of relative humidity, significant wave height, visibility, and stability parameter (z/L). When wind speed is greater than 15 m s^{-1}, the removal ratio of all variables increases (Fig. 6a). In the weak-wind range (<3 m s^{-1}), the removal ratios increase up to 80%. The error ratio of water vapor is correlated with significant wave height and increases as

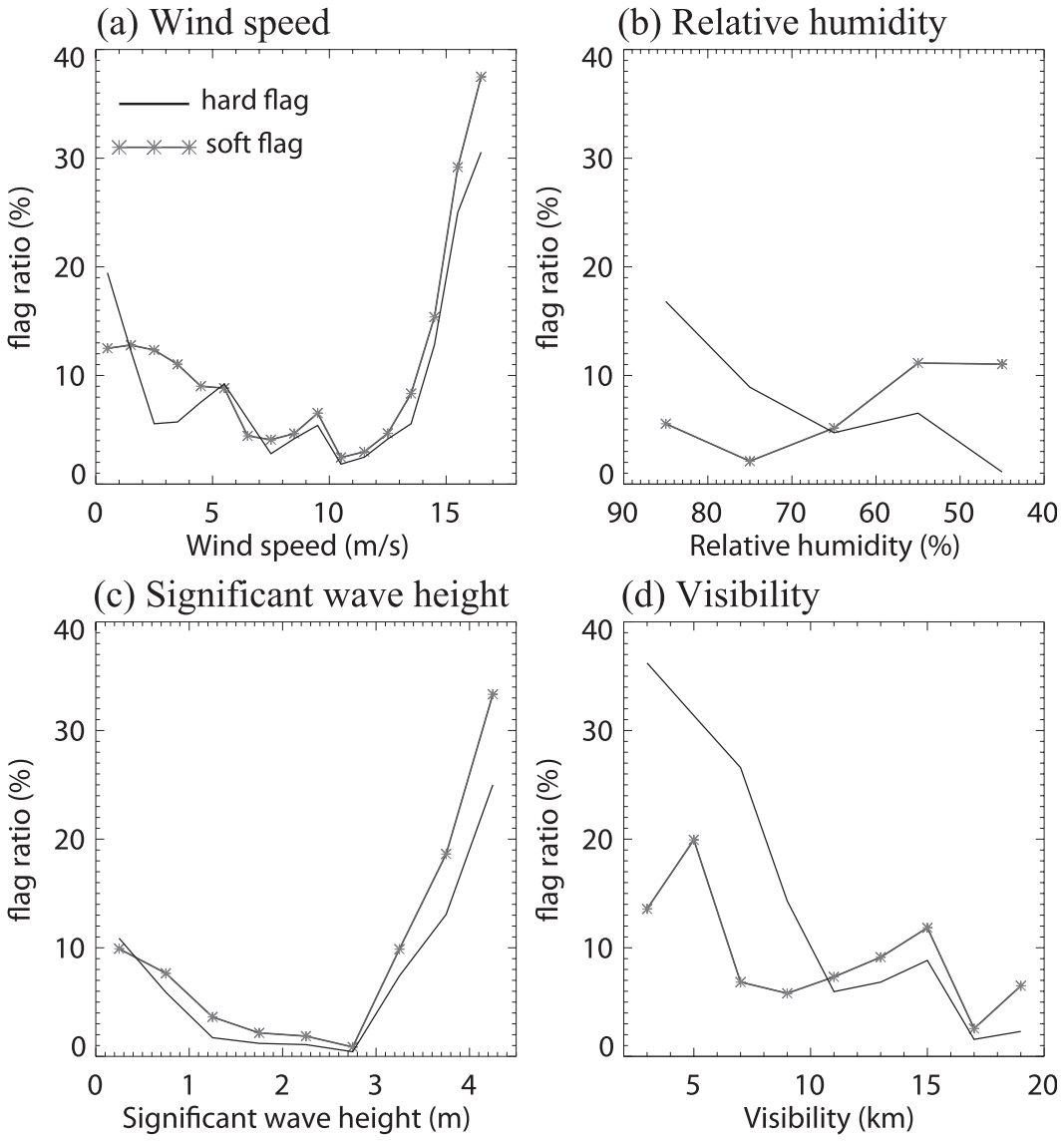

FIG. 4. The error-flag ratio of water vapor as a function of (a) horizontal wind speed, (b) relative humidity, (c) significant wave height, and (d) visibility. The solid black line indicates the hard-flagged error ratio and the solid gray line (asterisks) indicates the soft-flagged error ratio.

relative humidity increases (Figs. 6b,c). When visibility decreases, the error ratios of water vapor and air temperature increase (Fig. 6d). The error ratios for water vapor are larger in near-neutral and stable conditions (Fig. 6e). This result indicates that a significant portion of the latent heat flux data is eliminated. Bentamy et al. (2003) show some regional biases of latent heat flux in low wind conditions, where air–sea temperature differences and atmospheric stratification values are large. Because of the correlation between measurement problems and certain atmospheric conditions, bias in the distribution of the data is unavoidable.

4. Tilt correction

a. Methods

Three versions of the data are generated by applying the ''double rotation'' (DR), ''triple rotation'' (TR), and ''planar fit'' (PF) methods. The DR and TR approaches are applied to 30-min records while PF is applied to the entire dataset. The first rotation of the DR method rotates the mean wind in the horizontal plane into the wind direction such that $\overline{v}_S = 0$, while the second rotation rotates the mean wind vertically such that $\overline{w}_S = 0$. Here, the subscript S indicates wind observed from sonic

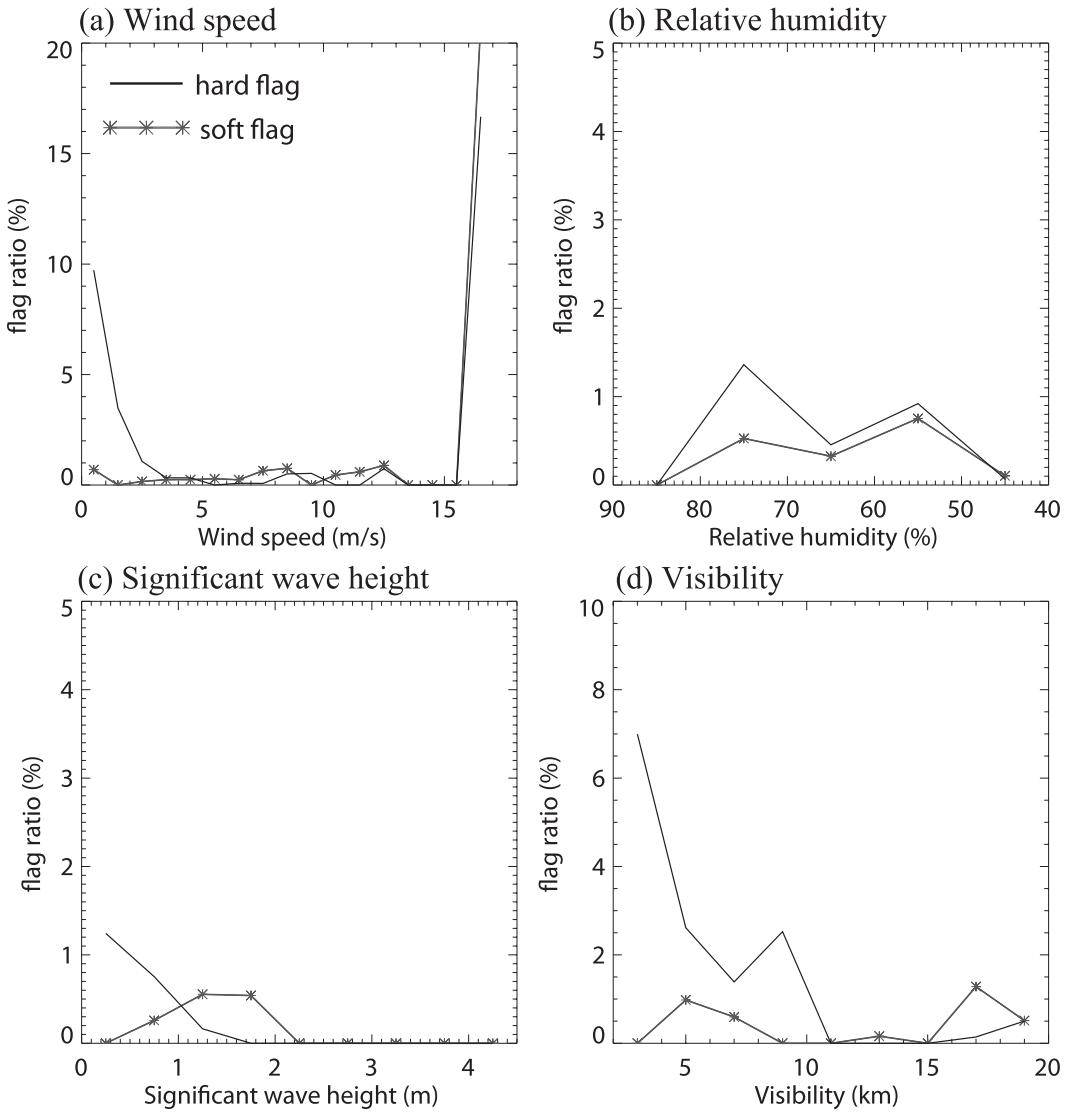

FIG. 5. Error flag ratio of w component wind as a function of (a) horizontal wind speed, (b) relative humidity, (c) significant wave height, and (d) visibility. The solid black line and solid gray line (asterisks) indicate the hard-flagged error ratio and the soft-flagged error ratio, respectively.

anemometer. In the TR method, a third rotation eliminates the lateral stress. As suggested by McMillen (1988), when the third rotated angle exceeds 10°, the third rotation is omitted because significant error occurs in this situation.

The PF method is utilized to obtain a two-dimensional plane, based on the multiple linear regressions of w against u and v using long-term measurements of these variables. The plane obtained here constitutes a long-term mean streamline coordinate system. The measured wind velocities are transformed into this long-term mean streamline coordinate system through rotation matrix $\mathbf{P}$ as given in Eq. (1):

$$\mathbf{U}_P = \mathbf{P}(\mathbf{U}_S - \mathbf{c}), \tag{1}$$

where $\mathbf{U}_S$ is the measured wind vector, $\mathbf{U}_P$ is the wind vector in a mean streamline coordinate system, and $\mathbf{c}$ is the mean offset in the measured winds due to instrument error. The matrix $\mathbf{P}$ is defined in terms of α (yaw angle) and β (pitch angle) as follows:

$$\mathbf{P} = \begin{pmatrix} \cos\alpha & 0 & -\sin\alpha \\ 0 & 1 & 0 \\ \sin\alpha & 0 & \cos\alpha \end{pmatrix} \begin{pmatrix} 1 & 0 & 0 \\ 0 & \cos\beta & \sin\beta \\ 0 & -\sin\beta & \cos\beta \end{pmatrix} = \begin{pmatrix} \cos\alpha & \sin\alpha\sin\beta & -\sin\alpha\cos\beta \\ 0 & \cos\beta & \sin\beta \\ \sin\alpha & -\cos\alpha\sin\beta & \cos\alpha\cos\beta \end{pmatrix}, \tag{2}$$

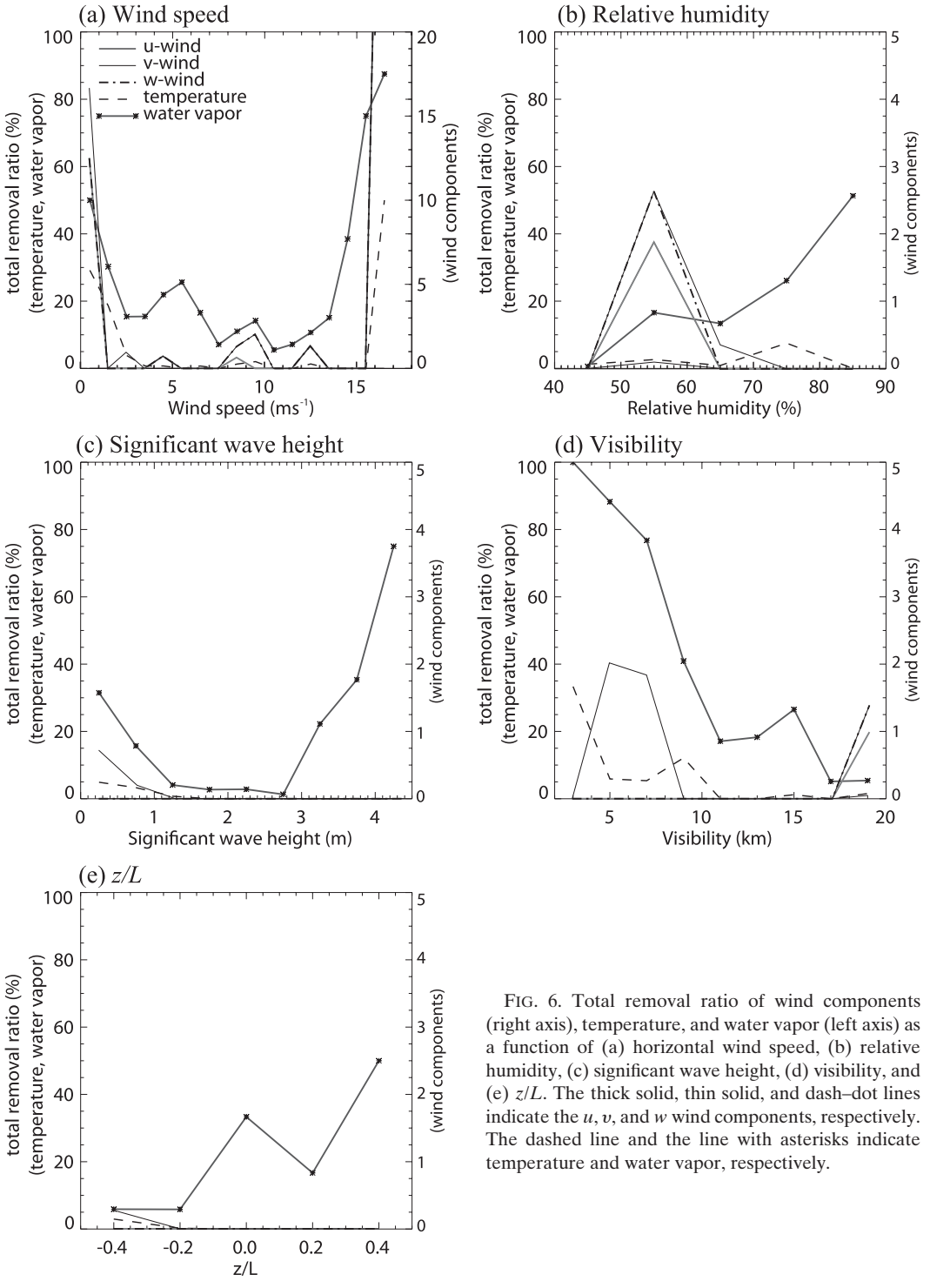

FIG. 6. Total removal ratio of wind components (right axis), temperature, and water vapor (left axis) as a function of (a) horizontal wind speed, (b) relative humidity, (c) significant wave height, (d) visibility, and (e) z/L. The thick solid, thin solid, and dash–dot lines indicate the u, v, and w wind components, respectively. The dashed line and the line with asterisks indicate temperature and water vapor, respectively.

where three matrix components (p_{31}, p_{32}, p_{33}) satisfy the following orthogonal condition:

$$p_{31}^2 + p_{32}^2 + p_{33}^2 = 1. \quad (3)$$

By expanding Eq. (1), the mean wind components can be written as follows:

$$\overline{u}_P = p_{11}(\overline{u}_S - c_u) + p_{12}(\overline{v}_S - c_v) + p_{13}(\overline{w}_S - c_w), \quad (4)$$

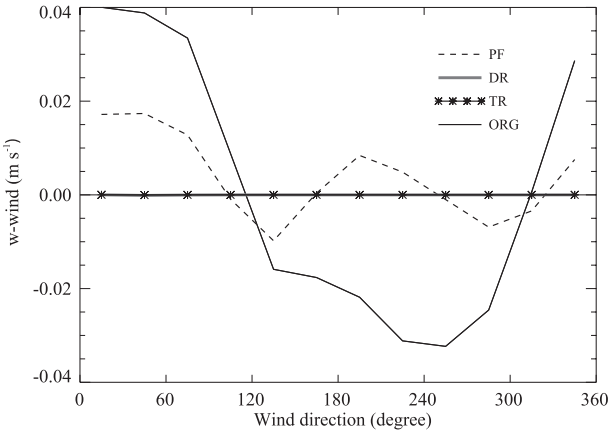

FIG. 7. Mean vertical motion for the uncorrected data (labeled ORG) and data corrected by PF, DR, and TR as a function of wind direction.

$$\overline{v}_P = p_{21}(\overline{u}_S - c_u) + p_{22}(\overline{v}_S - c_v) + p_{23}(\overline{w}_S - c_w), \quad (5)$$

and

$$\overline{w}_P = p_{31}(\overline{u}_S - c_u) + p_{32}(\overline{v}_S - c_v) + p_{33}(\overline{w}_S - c_w). \quad (6)$$

In the mean streamline coordinate system, where $\overline{w}_P$ is taken to be zero, Eq. (6) is reduced to the tilt correction, Eq. (7):

$$\begin{aligned}\overline{w}_S &= c_w - \frac{p_{31}}{p_{33}}(\overline{u}_S - c_u) - \frac{p_{32}}{p_{33}}(\overline{v}_S - c_v) \\ &= b_0 + b_1(\overline{u}_S - c_u) + b_2(\overline{v}_S - c_v). \end{aligned} \quad (7)$$

To find the b coefficients, we use the following to minimize the function S:

$$S = \sum(\overline{w}_i - b_0 - b_1\overline{u}_i - b_2\overline{v}_i)^2. \quad (8)$$

Differentiating S will determine to b coefficient and setting each partial derivative equal to zero results in the following three normal equations:

$$nb_0 + \left(\sum\overline{u}_i\right)b_1 + \left(\sum\overline{v}_i\right) = \sum\overline{w}_i, \quad (9)$$

$$\left(\sum\overline{u}_i\right)b_0 + \left(\sum\overline{u}_i^2\right)b_1 + \left(\sum\overline{u}_i\overline{v}_i\right)b_2 = \sum\overline{u}_i\overline{w}_i, \quad \text{and} \quad (10)$$

$$\left(\sum\overline{v}_i\right)b_0 + \left(\sum\overline{u}_i\overline{v}_i\right)b_1 + \left(\sum\overline{v}_i^2\right)b_2 = \sum\overline{u}_i\overline{w}_i. \quad (11)$$

Here, $\overline{u}_i$, $\overline{v}_i$, and $\overline{w}_i$ are the mean velocities for each data run and n is the number of data runs. We solve this matrix through singular value decomposition. The three coefficients obtained from the three equations constitute the linear regression of Eq. (7). Finally, the first rotation is performed for the three wind components given in Eqs. (4)–(6) to satisfy $\overline{v} = 0$. The solution of these three equations provides the linear regression of $\overline{u}_S$, $\overline{v}_S$, and $\overline{w}_S$.

The angle between the wind and stress vectors is computed as

$$\theta = \arctan\left(\frac{\overline{v'w'}}{\overline{u'w'}}\right), \quad (12)$$

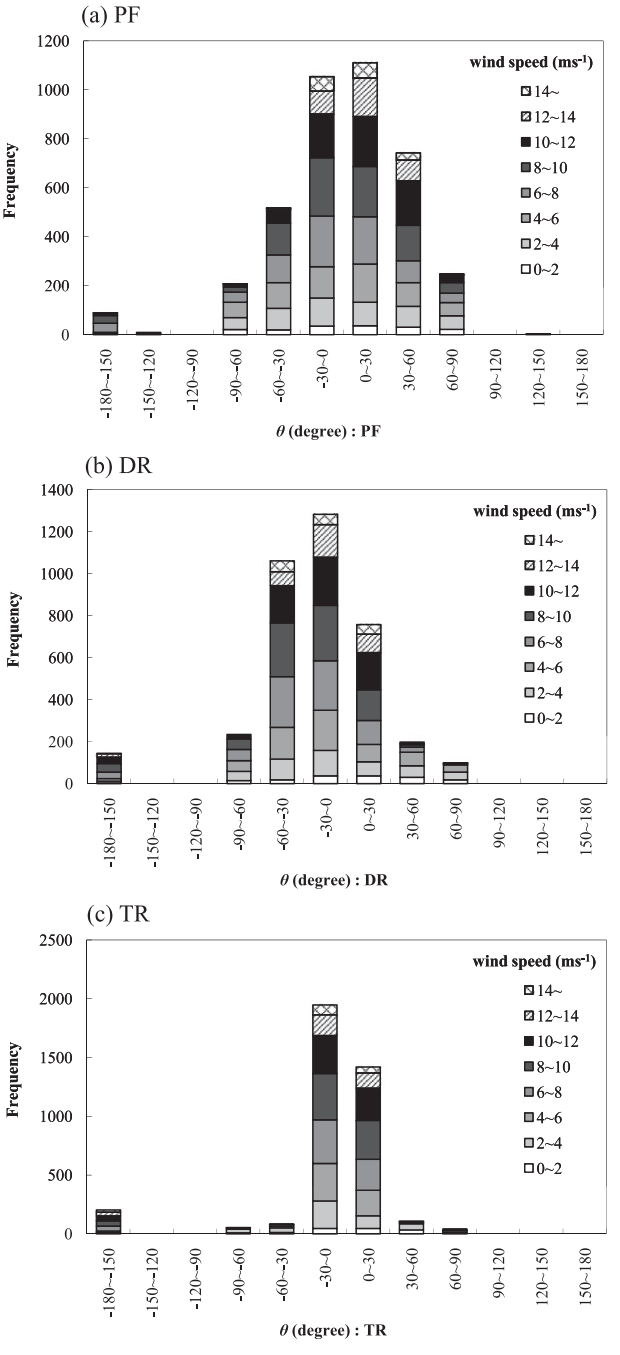

FIG. 8. Frequency distribution of the angle (θ) between stress vector and wind direction and the wind speed: (a) PF, (b) DR, and (c) TR.

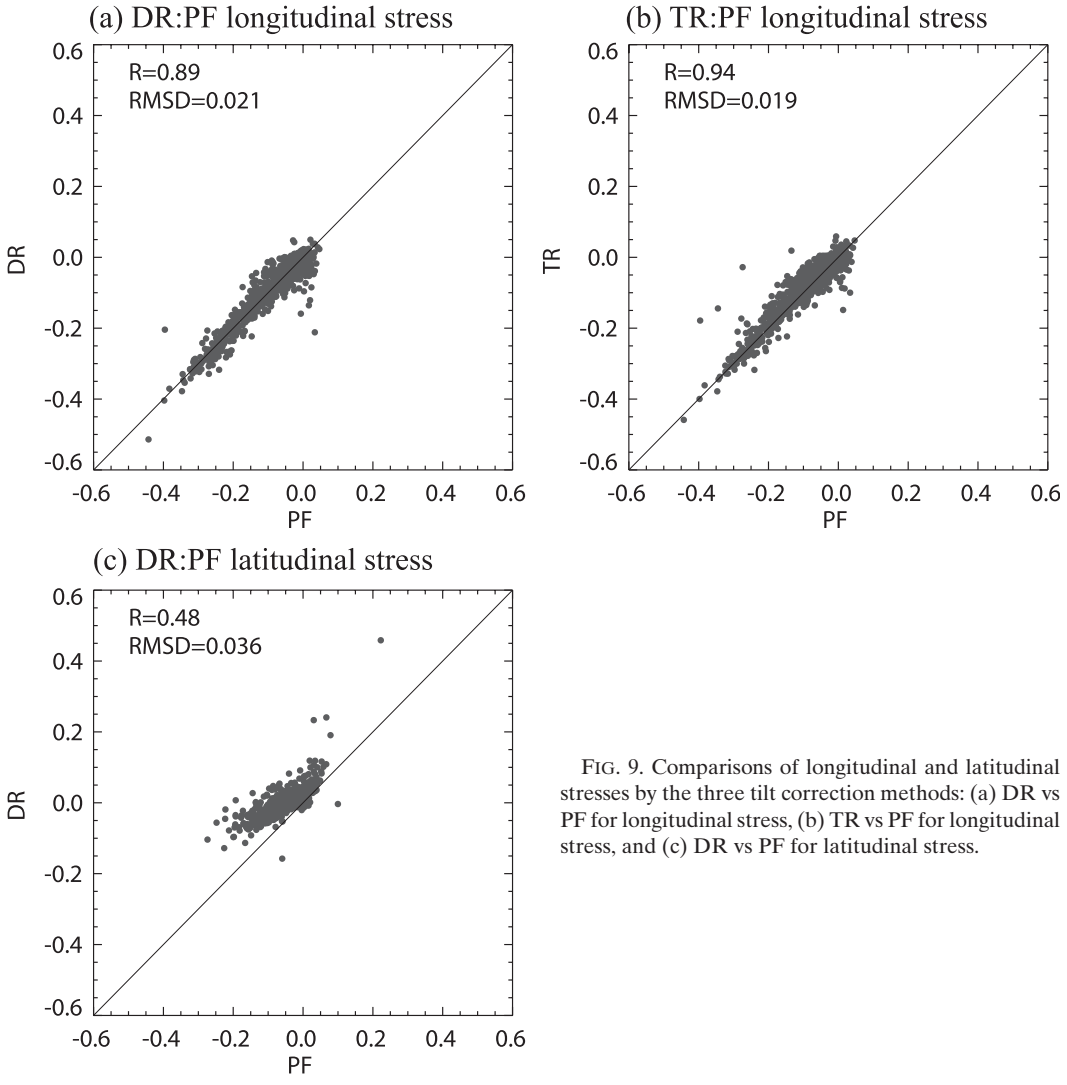

FIG. 9. Comparisons of longitudinal and latitudinal stresses by the three tilt correction methods: (a) DR vs PF for longitudinal stress, (b) TR vs PF for longitudinal stress, and (c) DR vs PF for latitudinal stress.

where positive angles represent orientation of the stress vector to the right of the wind vector.

The three tilt correction methods (DR, TR, and PF) described above are applied to the fast-response data observed with recording speed of 10 Hz. We compare the tilt correction methods in terms of the angle θ [Eq. (12)], the longitudinal stress, lateral stress, and turbulent fluxes in the next section.

b. Results of tilt rotations

The mean vertical motion for the uncorrected data reaches values of 3 cm^{-1} for the 240° wind direction sector (Fig. 7). Although significant, such vertical motions do not reveal large systematic trends anticipated as a result of the platform structure (large flow distortion). This may be due to the openness of the structure of the platform. The sharp change of mean vertical velocity with wind directions between 120° and 300° does suggest differences in the flow distortion between winds blowing through the structure and winds approaching the structure; sonic anemometer tilt is not expected to produce such sharp changes with wind direction.

The PF rotation substantially reduces the mean vertical motion (Fig. 7) even though it is not designed for flow distortion. No attempt was made to model the flow distortion of the platform because of its complex shape. The DR and TR methods eliminate the mean vertical motion for every record. The data corrected by DR are superimposed on the data corrected by TR.

Figure 8 shows the frequency distribution of the angle between the stress vector and wind direction and the wind speed, based on the DR, TR, and PF methods. The maximum frequency of occurrence is found at the angle interval between 0° and 30°. When the wind speed is

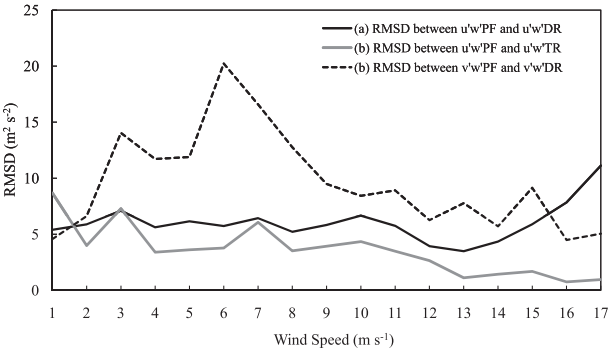

FIG. 10. The RMSD among three types of tilt correction methods (DR, TR, and PF) in terms of wind speed. The values are normalized by the square of PF stress: RMSD between the PF and DR for longitudinal stresses; RMSD between the PF and TR for longitudinal stresses; and RMSD between the PF and DR for latitudinal stresses.

strong, θ tends to be positive (stress vector directed to the right of the wind vector). This agrees with Ekman theory where at a given level, the shear vector, and therefore the stress vector, are directed to the right of the wind vector.

The plot in Fig. 8b depicts the frequency distribution of θ obtained by DR. In strong winds, the angle θ resulting from the DR method tends to be more negative (stress vector to the left of the wind vector). An isolated frequency peak occurs for stress approximately opposite to the wind direction for all three methods (Fig. 8). These cases correspond to momentum flux from the sea to the atmosphere. Since these situations generally occur with weak winds, they probably result from a swell moving faster than the wind (Grachev and Fairall 2001).

Figure 9 shows that the longitudinal stresses ($\overline{u'w'}$) resulting from each of the three methods are highly correlated. The lateral stresses ($\overline{u'w'}$) resulting from the DR method are greater than those from the PF method. The correlation coefficient between the two lateral stresses is only 0.48. Figure 10 shows the root-mean-square difference (RMSD) of longitudinal and lateral stresses from the DR and TR methods with respect to the PF method as a function of horizontal wind speed. The values are normalized in terms of the square of the PF stress. The normalized differences increase as wind speed decreases except the RMSD of longitudinal stress from the TR method. The latitudinal stress values differ

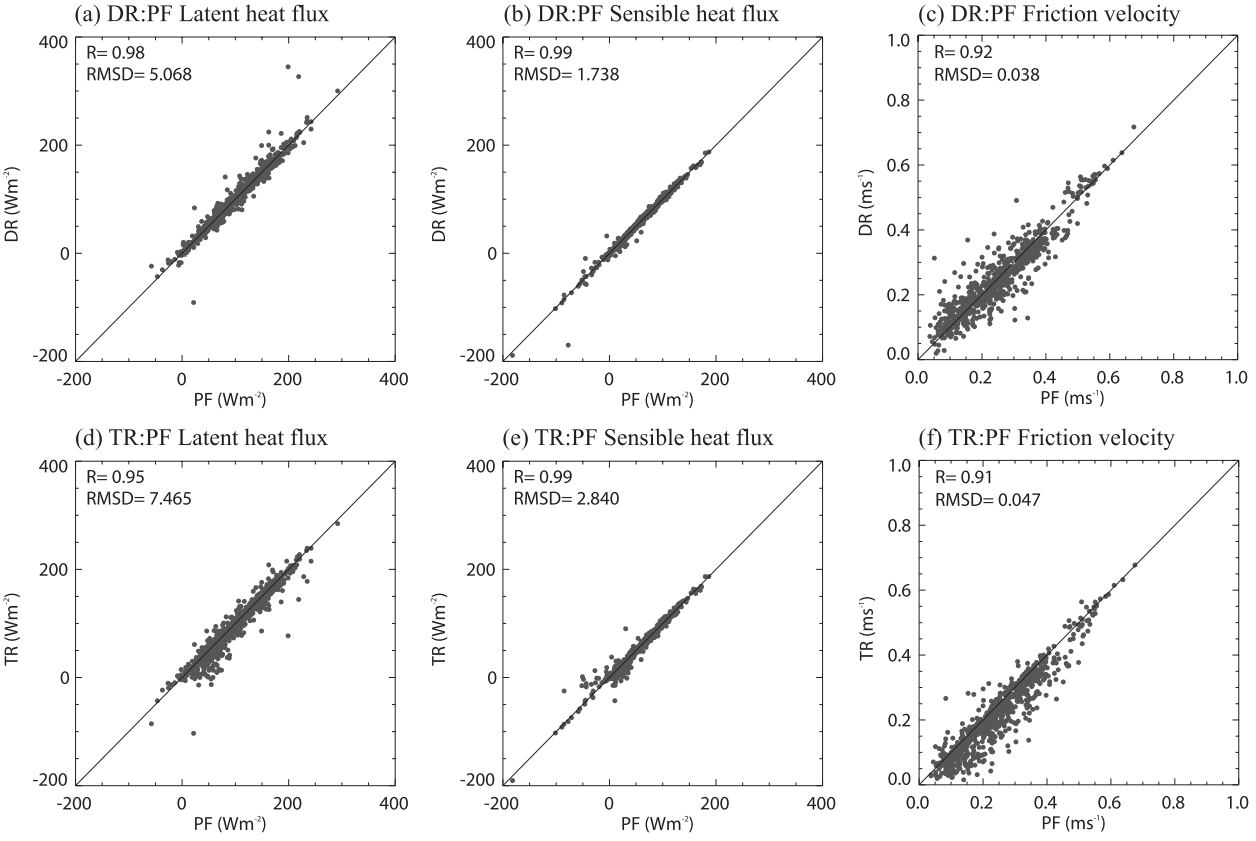

FIG. 11. (a) The DR vs PF for latent heat flux, (b) DR vs PF for sensible heat flux, (c) DR vs PF for friction velocity, (d) TR vs PF for latent heat flux, (e) TR vs PF for sensible heat flux, and (f) TR vs PF for friction velocity. The solid line represents 1:1.

more between methods. Since the different tilt rotations disagree and the ''correct'' tilt rotation is not known, attempts to physically interpret the lateral stress may be unjustified, both here and in previous studies.

In Fig. 11, the latent heat flux, sensible heat flux, and friction velocity from the DR and TR methods are compared with results from the PF method. The latent heat flux from the DR method is similar to that from the PF method (Fig. 11a) with a correlation of 0.98, while the coefficient between the values from the TR and the PF methods is 0.95. The sensible heat fluxes resulting from the three different methods are also highly correlated (Figs. 11b,e). Scalar fluxes are much less affected by the tilt rotation compared to the momentum flux, as is evident from the larger disagreement between estimates of the friction velocity (Figs. 11c,f). This disagreement is related mainly to differences between the different estimates of the lateral stress (Fig. 9).

5. Conclusions

Over the open ocean, direct turbulent flux measurements are more difficult than over land. This study analyzed the quality of fast-response data collected from an open ocean research platform. We investigated the dependence of fast-response instrument errors on atmospheric and oceanic conditions using the quality control algorithms of Vickers and Mahrt (1997) after removal of measurements taken in wind directions most likely influenced by flow distortion and removal of rain and high humidity conditions. The observation errors were flagged as hard (definite error) and soft (possible error). Hard-flagged errors most often occurred with strong or light winds, large significant wave height, large relative humidity, low visibility, and stable conditions. Water vapor errors were the most common in stable weak-wind conditions. Because of the correlation between significant instrument errors and weather conditions, analysis bias is unavoidable. The removal ratio is 1.6% for the u component, 2% for the v component, 7.2% for the w wind, 2.4% for air temperature, and 15.2% for water vapor in whole the quality control process.

Results from the three tilt correction methods (the double rotation, the triple rotation, and the planar fit methods) were compared. The longitudinal stress values from the DR, TR, and PF methods agreed reasonably well. However, significant differences of the lateral stresses between the different methods led to large differences in the angle between the wind and stress vectors. Although definite conclusions are not possible, the DR method seems more suitable since the TR method eliminates suspected true lateral stress and the PF method is not designed for the peculiarities of the flow distortion. Differences were greatest with weak winds. Since the ''best'' tilt rotation method cannot be established with certainty, the angle between the wind and stress vectors remains uncertain. Previous attempts to identify the physics of the lateral stress may have been compromised by uncertainties in the tilt rotation correction.

Acknowledgments. We thank the Korean Ocean Research and Development Institute for providing the data observed in the Ieodo ocean research station. This work was supported by Ministry of Environment as ''The Ecotechnopia 21 Project'' and Korean Ocean Research Development Institute as ''Construction of ocean research stations and their application studies.''

REFERENCES

Bentamy, A., K. B. Katsaros, A. M. Mestas-Nuñez, W. M. Drennan, E. B. Forde, and H. Roquet, 2003: Satellite estimates of wind speed and latent heat flux over the global oceans. *J. Climate,* **16,** 637–656.

Carter, D. J. T., 1982: Prediction of wave height and period for a constant wind velocity using the JONSWAP results. *Ocean Eng.,* **9,** 17–33.

Finnigan, J. J., R. Clement, Y. Malhi, R. Leuning, and H. A. Cleugh, 2003: A re-evaluation of long-term flux measurement techniques. Part I: Averaging and coordinate rotation. *Bound.-Layer Meteor.,* **107,** 1–48.

Foken, T., 1999: Comparison of the sonic anemometer Young Model 81000 during VOITEX-99. University of Bayreuth Dept. of Micrometeorology Deliverable 8, 12 pp.

——, and B. Wichura, 1996: Tools for quality assessment of surface-based flux measurements. *Agric. For. Meteor.,* **78,** 83–105.

——, U. Weisensee, H.-J. Krizel, and V. Thierman, 1997: Comparison of new type sonic anemomters. *Proc. 12th Symp. on Boundary Layer and Turbulence,* Vancouver, BC, Canada, Amer. Meteor. Soc., 356–357.

Friehe, C. A., S. P. Burns, D. Khelif, and X. Song, 1996: Meteorological and flux measurements from the NOAA WP3D aircraft in TOGA COARE. *Proc. Eighth Conf. on Air–Sea Interaction and Conference on the Global Ocean–Atmosphere–Land System,* Atlanta, GA, Amer. Meteor. Soc., 42–45.

Geernaert, G. L., 1983: Variation of the drag coefficient and its dependence on sea state. Ph.D. thesis, University of Washington, 120 pp.

Grachev, A. A., and C. W. Fairall, 2001: Upward momentum transfer in the marine boundary layer. *J. Phys. Oceanogr.,* **31,** 1698–1711.

——, ——, J. E. Hare, J. B. Edson, and S. D. Miller, 2003: Wind stress vector over ocean waves. *J. Phys. Oceanogr.,* **33,** 2408–2429.

Højstrup, J., 1993: A statistical data screening procedure. *Meas. Sci. Technol.,* **4,** 153–157.

Johansson, C., A.-S. Smedman, U. Högström, J. G. Brasseur, and S. Khanna, 2001: Critical test of the validity of Monin–Obukhov similarity during convective conditions. *J. Atmos. Sci.,* **58,** 1549–1566.

Kaimal, J. C., and J. J. Finnigan, 1994: *Atmospheric Boundary Layer Flows: Their Structure and Measurement*. Oxford University Press, 289 pp.

Kinsman, B., 1965: *Wind Waves*. Prentice-Hall, 676 pp.

Korea Ocean Research and Development Institute, 2001: Construction and operation of the Ieodo ocean observation station. R&D report of Ministry of Maritime Affairs and Fisheries.

Kraan, C., and W. A. Oost, 1989: A new way of anemometer calibration and its application to a sonic anemometer. *J. Atmos. Oceanic. Technol.,* **6,** 516–524.

Mahrt, L., 1991: Eddy asymmetry in the sheared heated boundary layer. *J. Atmos. Sci.,* **48,** 472–492.

Mauder, M., C. Liebethal, M. Göckede, J.-P. Leps, F. Beyrich, and T. Foken, 2006: Processing and quality control of flux data during LITFASS-2003. *Bound.-Layer Meteor.,* **121,** 67–88.

——, and Coauthors, 2007: The Energy Balance Experiment EBEX-2000. Part II: Intercomparison of eddy-covariance sensors and post-field data processing methods. *Bound.-Layer Meteor.,* **123,** 29–54.

McMillen, R. T., 1988: An eddy correlation technique with extended applicability to non-simple terrain. *Bound.-Layer Meteor.,* **43,** 231–245.

Paw U, K. T., D. D. Baldocchi, T. P. Meyers, and K. B. Wilson, 2000: Correction of eddy-covariance measurements incorporating both advective effects and density fluxes. *Bound.-Layer Meteor.,* **97,** 487–511.

Pospelov, M. N., and Coauthors, 2009: Air–sea interaction in a coastal zone: The results of the CAPMOS'05 experiment on an oceanographic platform in the Black Sea. *Atmos. Res.,* **94,** 61–73.

Sun, J., 2007: Tilt corrections over complex terrain and their implication for CO_2 transport. *Bound.-Layer Meteor.,* **124,** 143–159.

Tanner, C. B., and G. W. Thurtell, 1969: Anmoclinometer measurements of reynold stress and heat transport in the atmospheric surface layer. Department of Soil Science, University of Wisconsin, Madison, WI, Research and Development Tech. Rep., ECOM 66-G220F, 82 pp.

Thomson, B. E., and R. C. Hassman Jr., 2001: Meteorological twin-hot-film anemometry. *J. Atmos. Oceanic. Technol.,* **18,** 493–502.

Tucker, M. J., and E. G. Pitt, 2001: *Waves in Ocean Engineering*. Elsevier, 550 pp.

Vickers, D., and L. Mahrt, 1997: Quality control and flux sampling problems for tower and aircraft data. *J. Atmos. Oceanic. Technol.,* **14,** 512–526.

Wilczak, J. M., S. P. Oncley, and S. A. Sage, 2001: Sonic anemometer tilt correction algorithms. *Bound.-Layer Meteor.,* **99,** 127–150.

Yim, J.-W., K.-R. Lee, J.-S. Shim, and C.-A. Kim, 2006: Numerical study on the observational error of sea surface winds at Ieodo ocean research station. *J. Korean Soc. Coastal Oceanic Eng.,* **18,** 189–197.